ADVANCED MATERIALS
www.advmat.de

Rational Design of Color-Pure Blue Organic Emitters by Poly-Heteroaromatic Omni-Delocalization

Sunwu Song, Siyang Feng, Liangxuan Wang, Jinwon Jun, Begoña Milián-Medina, Reinhold Wannemacher, Jaesang Lee, Min Sang Kwon, and Johannes Gierschner**

Current research on organic light emitters which utilize multiple resonance -induced thermally activated delayed fluorescence (MR-TADF) materials is gaining significant interest because of the materials' ability to efficiently generate color-pure blue emission. However, the underlying reasons for high color purity remain unclear. It is shown here that these emitters share a common electronic basis, which is deduced from resonance structure considerations following Clar's rule, and which is termed as "poly-heteroaromatic omni-delocalization" (PHOD). The simple and clear design rules derived from the PHOD concept allow extending the known chemical space by new structural motifs. Based on PHOD, a set of novel high-efficiency color-pure emitters with brilliant deep-blue hue is specifically designed.

S. Song, M. S. Kwon
Department of Materials Science and Engineering
Research Institute of Advanced Materials
Seoul National University
Seoul 08826, Republic of Korea
E-mail: minsang@snu.ac.kr

S. Feng, L. Wang, R. Wannemacher, J. Gierschner
Madrid Institute for Advanced Studies
IMDEA Nanoscience, C/ Faraday 9
Ciudad Universitaria de Cantoblanco
Madrid 28049, Spain
E-mail: johannes.gierschner@imdea.org

L. Wang
Institute of Physical and Theoretical Chemistry
Eberhard Karls University Tübingen
Auf der Morgenstelle 18, 72076 Tübingen, Germany

J. Jun, J. Lee
Department of Electrical and Computer Engineering
Inter-University Semiconductor Research Center
Seoul National University
Seoul 08826, Republic of Korea

B. Milián-Medina
Department for Physical Chemistry
Faculty of Chemistry
University of Valencia
Burjassot, Valencia 46100, Spain

The ORCID identification number(s) for the author(s) of this article can be found under https://doi.org/10.1002/adma.202404388

DOI: 10.1002/adma.202404388

1. Introduction

Research into multiple resonance-induced thermally activated delayed fluorescence (MR-TADF) materials has become a significant focus within the field of organic light emitting diodes (OLED) due to their potential for efficient deep blue emission;[1–7] within the OLED architecture, these blue emitters are used as fluorescence sensitizers, now often termed as "hyperfluorescent" materials.[8–10] Their unsurpassed color purity is particularly crucial, as it enables the development of ultra-high-definition OLED displays,[11] featuring exceptional realism and color reproduction, all without the need for color filters. Consequently, this simplifies the device structure and enhances energy efficiency. Since the Hatakeyama group reported **DABNA-1** as an ultrapure blue emitter in 2016,[12] the design of color-pure blue emitters has primarily relied on **DABNA-1** analogues with modest structural variations,[1–7] see **Scheme 1**.

Fundamentally, the main parameter for spectral broadening is effective coupling of vibrational modes.[16–19] Therefore, narrow emission bandwidths require the reduction of geometry change in the molecular core structure upon electronic de-excitation; this concerns in particular the bond lengths (Δ_{BL}), and bond length (BL) alternation along the conjugated path in alternating systems (Δ_{BLA}).[20,21] This was also realized in the context of DABNA-type emitters,[22] and vibronic coupling patterns of selected compounds were explicitly calculated.[22–25] However, the underlying electronic reasons for the small Δ_{BL} were not elucidated, while this is key for the envisaged targeted design of color-pure emitters.

In this work, we deduce the unreported underlying concept for small Δ_{BL} in narrow-band blue emitters, based on resonance structure considerations following Clar's rule, and which is termed as "poly-heteroaromatic omni-delocalization" (PHOD). This allows to formulate clearly defined simple design rules, which pave the way for targeted design of narrow-band emitters, expanding the known structural chemical space; such versatility may be important to enhance (temporal) stability of host-guest interactions in the device. Following these guidelines, we introduce a novel structural motif to design new compounds **DOBFT**, **DOBFIT** (Scheme 1), which provide high-efficiency color-pure emitters with a brilliant deep blue hue.

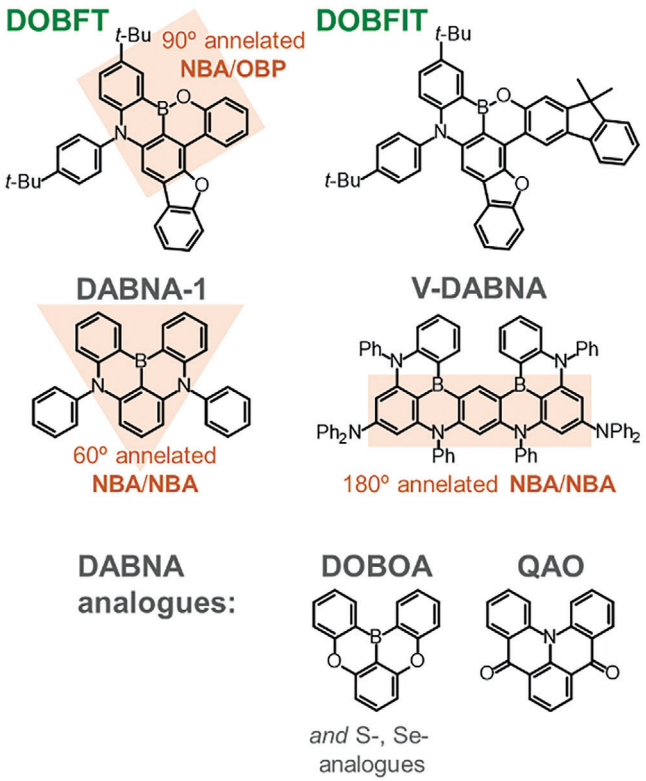

Scheme 1. Molecular structures of novel compounds **DOBFT**, **DOBFIT**, along with **DABNA-1**,[12] an extended structure (**V-DABNA**)[13] and analogues **DOBOA**,[14] **QAO**;[15] annelated **NBA**/**OBP** and **NBA**/**NBA** units are indicated (with annelation angle); for details see text.

2. Spectral Narrowing

Phenomenologically, the most commonly used parameters to characterize spectral properties (color and color purity) are λ_{max}, and the full width at half maximum (FWHM), usually given in nanometers; in any case, in order to secure that numbers can be properly compared, we will provide them as well in energy values (eV). Furthermore, we note that both parameters (λ_{max}, FWHM) can be misleading for vibronically structured spectra, as we will discuss in a forthcoming perspective. Therefore, we will additionally use more robust parameters to characterize the spectra, that is the weighted mean $\bar{E}$ of the emission spectrum I(E)

$$\bar{E} = \frac{\int E \cdot I(E)\, dE}{\int I(E)\, dE} \tag{1}$$

where I(E) is obtained from the spectrum recorded in λ under variable substitution as $I(E) = I(\lambda)\cdot\lambda^2$ (to ensure equal areas). Furthermore, from the variance σ_E^2 of the spectrum

$$\sigma_E^2 = \frac{\int (E-\bar{E})^2 \cdot I(E)\, dE}{\int I(E)\, dE} \tag{2}$$

the effective width γ_E can be defined; this reads, in analogy to the Gaussian width γ_G, as

$$\gamma_E = 2\sqrt{2\ln 2}\cdot\sigma_E \tag{3}$$

being indeed a robust measure for color pureness.

From vibronic coupling (VC) theory,[16–19] a normal mode of vibration is effective, if the nuclear motion coincides with the geometry change upon electronic de-excitation from the lowest excited state to the ground state, $S_1 \rightarrow S_0$. This gives rise to a Franck-Condon (FC) progression, and, in a multi-mode picture, to intercombinations, being convolutions of the individual FC progressions. This geometry change is induced by the change in the electronic structure, which concerns essentially the conjugated core with π, π^*-type frontier molecular orbitals (FMOs). VC to a symmetry-allowed transition can take place by (i) linear coupling (LC) of symmetry-allowed in-plane modes, both in the low-frequency (50–700 cm^{-1}; mainly carbon core deformations), and high-frequency domain (1200–1700 cm^{-1}; mainly C—C stretching), and by (ii) quadratic coupling (QC) via thermal activation of low-frequency out-of-plane modes (5–50 cm^{-1}; mainly torsions). These contributions have been disentangled by us in the past on vastly different systems.[20,21,26–31]

The coupling efficiency is quantified by the reorganization energy E_{re}, which correlates with the spectral width, and which corresponds to the difference between the adiabatic and vertical energies

$$E_{re} = E_{00} - E_{vert} \tag{4}$$

where E_{vert}, as the most probable energy of transition, corresponds to $\bar{E}$,[20] see Equation (1). For mirror symmetrical absorption and emission, E_{00} corresponds to the intersection between the spectra.[33]

Furthermore, optical spectra are broadened by environmental effects, mainly due to static and dynamic variations of the polarizability of the host environment close to the emitter; this is difficult to quantify,[31,34] and can be little influenced under practical conditions, in particular in devices. Nevertheless, the effect is quite invariant for weakly polar molecules in disordered nonpolar environments at room temperature, resulting in a Gaussian-shaped convolution function with a width γ_G of about 500–600 cm^{-1} (≈0.07 eV; see the Experimental Section);[21] this broadening typically leads to a collapse of the complex vibronic fine structure to one "apparent" progression.[20]

Therefore, central task to obtain narrow emission is to reduce the geometry change upon electronic (de)excitation; the main parameter herein is Δ_{BLA} within the carbon core.[20,21] The latter is often (however not always) directly related to the topologies imposed by the highest (lowest) (un)occupied MOs, i.e., HOMO (LUMO), which frequently constitute the $S_1 \rightarrow S_0$ transition. An illustrative example for strong Δ_{BLA} is stilbene, where the main geometry change takes place in the vinylene unit; here, S_0 exhibits strong BLA, here dictated mainly by the HOMO topology, while S_1 shows small BLA, reflecting a more polar character as the LUMO exhibits a quinoid topology, see **Figure 1** and the Experimental Section for details. Thus, in-plane bending and stretching modes couple efficiently by LC. At the same time, the strong Δ_{BLA} largely increases the frequency of the out-of-plane

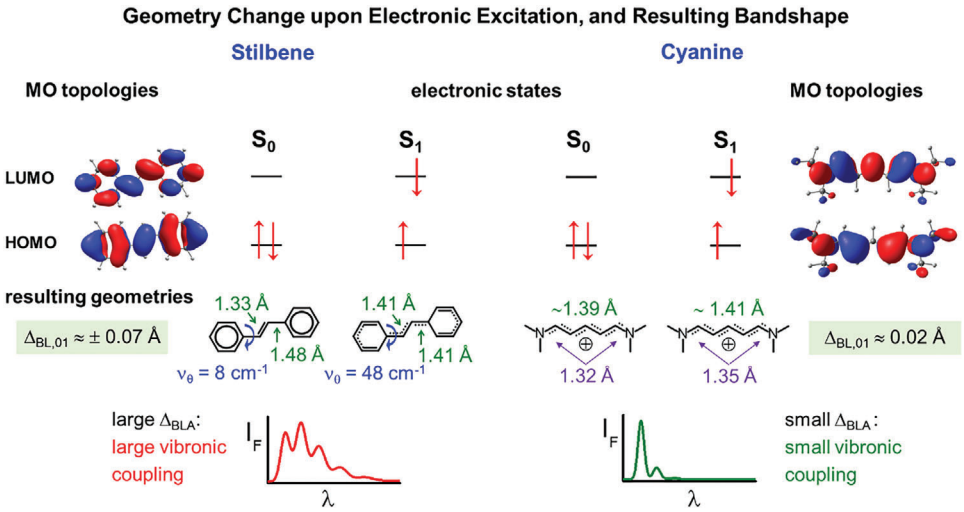

Figure 1. Vibronic coupling in stilbene and a model cyanine. DFT-calculated MO topologies and resulting geometries in ground and first excited singlet states (S_0, S_1) with relevant C—C (green) and C—N (violet) bond lengths (and, for stilbene, torsional frequencies; in blue[38]); resulting emission bandshapes (red, green; schematic).

torsional modes in S_1, giving rise to significant QC.[20] It is noted that QC in such polyene-like structures can be effectively reduced through rigid environments,[20,30–32] or by using rigidified structures,[27,28] as, e.g., in oligoacenes[35,36] or -thioacenes.[27] In these compounds, much higher vibronic resolution is observed compared to floppy structures (as in stilbene); however, LC is only little affected by rigidification, giving rise to still considerable E_{re}, reflected in very significant vibronic side bands.

One recipe to reduce Δ_{BL} is to move from polyene-like structures (as in stilbene) to cyanine (polymethine) structures, as here the resonance structures are identical. Therefore, the BLA is already small in S_0, and, consequently, remains small in S_1 (Figure 1). This is reflected in narrow spectral shapes for cyanine dyes, due to largely reduced LC and QC.[21] Nevertheless, the cyanine recipe is not viable for pure blue emitters, as cyanines emit in the green to (deep) red spectral range,[39] due to the inevitable low-lying S_1 state as imposed by the cyanine structure.[40]

3. The PHOD Concept

Therefore, the recipe to generate small Δ_{BL} for blue emitters has to be chosen on a different basis. In fact, a known possibility to reduce the BLA in the ground state is to make use of Clar's rule; the latter states that in polycyclic aromatic hydrocarbons the resonance structure (RS) with the highest number of disjoint delocalized π-sextets is the most relevant for the properties (e.g., reactivity).[41,42] For instance, in anthracene (a linear annelated aromatic "acene"),[35,43] from the four RS only one (moving) Clar sextet is observed, see **Figure 2**. On the other hand, in the π-isoelectronic phenanthrene (an angular annelated aromatic "phene"),[35,43] five RS and two Clar sextets can be formulated in the outer rings (β, β', see Figure 2). As well established in resonance theory, this directly impacts geometry.[41,42] In fact, bond orders can be estimated from the RS,[42] and, with a few reasonable assumptions (see the Experimental Section), bond lengths; indeed, the latter agree well with the density functional theory (DFT) calculations (Tables S2 and S5, Supporting Information). According to the bond lengths, anthracene shows significant BLA in the outer rings (Figure 2; Tables S2 and S5, Supporting Information), whereas in phenanthrene the outer rings are predominantly delocalized. Still, in the central ring (α) of phenanthrene, significant BLA is observed. Therefore, it is not expected that, upon electronic excitation, Δ_{BL} in phenanthrene is significantly smaller than in anthracene; this is indeed confirmed in the (TD)DFT calculations and in the experimental UV–vis spectra.[35,37] Furthermore, even for a larger number of rings, the HOMO→LUMO excitation of phenes remains in the UV range.[35,43] Thus, reduction of the BLA in the connecting rings is key to obtain a predominant delocalized character here as well; this can be indeed achieved by proper substitution.

For this, we first consider di-substitution in the 9,10-positions with X = BH or NH (it is noted that these systems are not isoelectronic to the acenes). The calculations now predict predominant delocalized outer rings, both for the substituted phenanthrene as well as anthracene, while the central ring has mainly single bond character, see Table S5 (Supporting Information); accordingly, non-negligible Δ_{BL} upon electronic excitation is expected. Therefore, in the next step, we consider an isoelectronic (and isosteric) anthracene analogue, i.e., 9,10-azaboraanthracene (**NBA**), see Figure 2. Here, four neutral RS can be formulated, as well as four zwitterionic RS; the latter are expected to contribute significantly, as they are promoted by the electron deficient character of B and the electron rich character of N in *para*-position to each other.[44] The neutral RS give rise to two Clar sextets, which results in a predominant delocalized character in the outer rings. On the other hand, as the good agreement between DFT and simple RS estimations clearly evidences (Table S2, Supporting Information), the zwitterionic RS provide equally predominant delocalized character of B—C and N—C bonds in the central azaborine ring. In fact, all calculated C—C bonds are less than |±0.02 Å| with respect to an averaged single/double bond (1.40 Å; see the Experimental Section), and similarly for C—B and C—N bonds; see Figure 2 and Table S2 (Supporting Information). Upon electronic excitation, most of the bonds experience

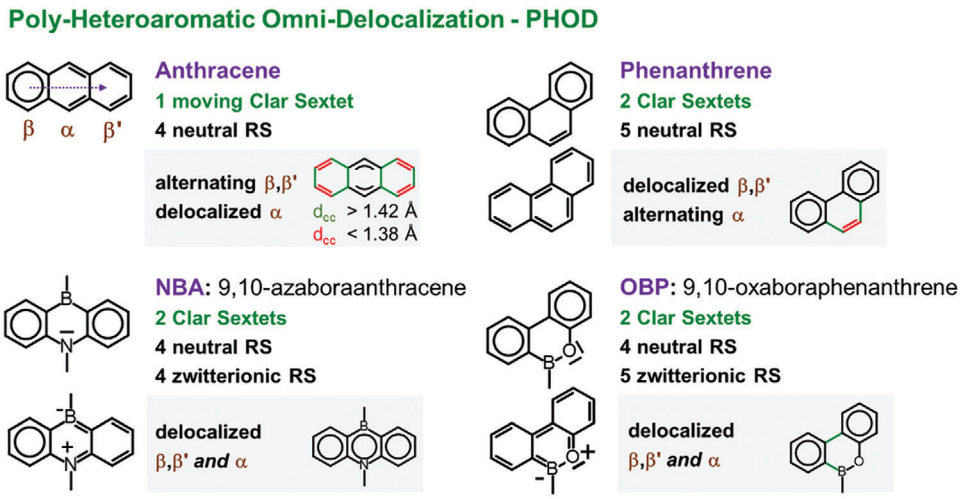

Figure 2. Formulation of the PHOD Concept, depicting anthracene and phenanthrene, and the 9,10-hetero-analogues **NBA** and **OBP**. Resonance structures (RS) and corresponding Clar sextets. The gray-shaded structures correspond to the resulting DFT-calculated geometries; where predominantly delocalized bonds are given in black (1.38 Å ≤ C—C ≤ 1.42 Å; 1.45 Å ≤ C—B ≤ 1.53 Å; 1.32 Å ≤ C—N ≤ 1.39 Å; 1.26 Å ≤ C—O ≤ 1.33 Å; 1.35 Å ≤ B—O ≤ 1.43 Å); red (green) bond color indicate predominant double (single) bond character.

only small changes Δ_{BL} of about ±0.01 Å, while only two bonds are elongated by 0.03 Å (Table S5, Supporting Information). The small Δ_{BL} is due to the small changes in the bonding characteristics of each individual bond upon excitation; see the Experimental Section for details, and the MO topologies in Figure S10 (Supporting Information). In all, this suggests small E_{re} and thus narrow emission for **NBA**. In fact, **NBA** serves as the central motif of **DABNA-1**, and its extensions,[13,45] alongside with analogues of N:B such as O:B,[14] S:B, Se:B or N:CO,[15,46] in other color-pure DABNA-type blue emitters (Scheme 1).[1–7] This constitutes a general design concept, which we term as "poly-heteroaromatic omni delocalization" (PHOD). Besides this central structural feature, which largely reduces Δ_{BL} against the acene family, it also breaks the symmetry of the un-/occupied MOs (minimizing alternant pairing effects; see the Supporting Information for details), and reduces the HOMO–LUMO gap toward the blue spectral region.

The PHOD concept allows to design new structural motifs; in fact, applying the concept to phenanthrene, one obtains 9,10-azaboraphenanthrene (**NBP**),[47] or its oxa-analogue **OBP**,[48] see Figure 2. Although PHOD in these compounds shows up in a similar manner as in **NBA**, we note predominant single bond character in the interring C—C bond as well as in the C—B bond; this is due to the fact that only in one of the nine RS these bonds exhibit double bond character. Therefore, we expect a modest increase of the spectral width compared to **NBA**. On the other hand, the new motifs allow to extend the core structure; in fact, while **NBA** allows extension only in a linear fashion, or angular by 60° (as in **DABNA-1**), **OBP** or **NBP** allow for angular annelation at 90°, see Scheme 1. This enhances structural versatility and enables precise color tuning, as we will see below. Moreover, it is important to note that the use of multiple **NBA**, **NBP**, **OBP** motifs increases the number of zwitterionic resonance structures and with this the delocalization in the heteroaromatic rings. For instance, going from **NBA** to the **DABNA** core structure, the percentage of zwitterionic structures increases from $x_{ZI} = 4/8 = 50\%$ (Figure 2) to $x_{ZI} = 16/24 = 67\%$, see Scheme S3 (Supporting Information). For the combined **NBA**/**OBP** motifs, being the core structure of **DOBFT**, **DOBFIT** (Scheme 1), x_{ZI} yields 18/26 = 69%, as compared to **OBP** with $x_{ZI} = 5/9 = 55\%$; see Scheme S3 (Supporting Information).

Therefore, utilizing the PHOD concept, the recipe for efficient pure blue fluorophores can be formulated as follows: to (i) maintain a rigid core structure, to (ii) avoid direct annelation of benzene moieties, but instead co-annelation via **NBA** or **NBP**/**OBP** motifs, to (iii) extend the core structures by using multiple **NBA**/**NBP**/**OBP** motifs, to (iv) fine-tune the properties by further substitution/annelation, but to avoid hereby (v) structures with dominant BLA, and (vi) excessive long-range CT character.

4. PHOD-Based Design of Novel Color-Pure Blue Emitters

In this spirit, we have designed two novel molecular structures, **DOBFT** and **DOBFIT** (see Scheme 1; for full name and synthesis, see the Experimental Section and Supporting Information). These structures incorporate, for the first time, the **OBP** motif besides **NBA**. This enlarges the available structural versatility by a new type of 90°-angular annelation; additional bulky *tert*-butyl side groups suppress π–π stacking; this largely improves the solubility, and increases the material stability for OLED applications.[49,50] The core structure allows for the formulation of four (**DOBFT**) and five (**DOBFIT**) Clar sextets (benzene moieties), which fine-tunes the optical properties, vide infra. The resulting emitting S_1 state of **DOBFT** (corresponding to the HOMO→LUMO excitation), provides a moderate oscillator strength $f_{01} = 0.22$ with partial CT character, see **Figure 3** and Table S4 (Supporting Information). The absence of substantial QC, due to the rigid core structure, is in particular visible in the mirror symmetry between the vibronically structured absorption and emission spectra,[20,28] see **Figure 4**. Thus, E_{00} can be precisely determined from the intersection of absorption and

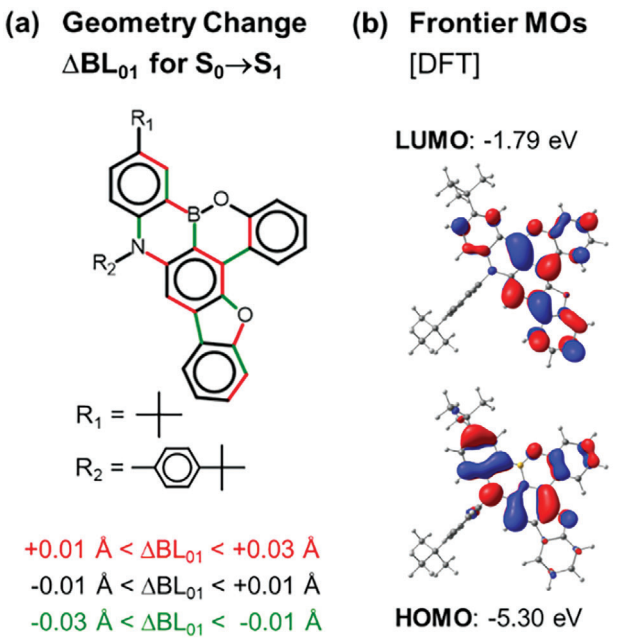

Figure 3. Geometrical and electronic properties of the **DOBFT** core structure. a) (TD)DFT calculated geometry change Δ_{BL} = BL(S_1)-BL(S_0); b) HOMO and LUMO energies and topologies.

emission at 2.87 eV (432 nm), see **Table 1**. The emission peaks at 2.84 eV (436 nm) in the first subband (F_1), and E_{vert} is determined to be 2.75 eV (451 nm) from Equation (1). Hence, E_{re} amounts to 0.12 eV via Equation (4); the low value for E_{re} directly reflects the narrow nature of emission. In fact, the F_2 subband (separated from F_1 by 0.15 eV) is significantly lower in intensity, i.e., $F_2/F_1 = 0.46$. The FWHM is therefore very small, determined to be 0.11 eV (16 nm). Similar considerations apply for **DOBFIT**, with λ_{max} = 441 nm, λ_{vert} = 456 nm, and with an even reduced FWHM of 0.09 eV (15 nm), see Table 1. Along with a few other compounds,[1–7] these are the lowest widths reported so far, representing the practical expected minimum. Nevertheless, as we emphasized above, the effective width γ_E is significantly larger than FWHM, giving in fact γ_E = 0.30 eV for **DOBFT** (0.29 eV for **DOBFIT**), see Table 1. This is larger than in **DABNA-1** (0.24 eV; Table 1), corresponding to somewhat superior color pureness of the latter. In any case, **DOBFT** and **DOBFIT** emit a brilliant blue hue, whose appearance in daylight under UV irradiation perfectly match their CIE coordinates, see Figure 4.

Table 1. Spectroscopic parameters of the compounds under study in toluene solution.

		DOBFT		DOBFIT		DABNA-1	
		E [eV]	λ [nm]	E [eV]	λ [nm]	E [eV]	λ [nm]
E_{00} [a]		2.87	432	2.84	437	2.78	446
E_{max}		2.84	436	2.81	441	2.74	453
E_{vert} [b]		2.75	451	2.72	456	2.67	465
E_{re} [c]		0.12		0.12		0.11	
FWHM		0.11	16	0.09	15	0.14	23
γ_E [d]		0.30		0.29		0.24	
CIE	x	0.150		0.147		0.140	
	y	0.045		0.053		0.058	
Φ_F [e]		0.92		0.96		0.94	
τ_F / ns [f]		8.1 (6.2)		6.3 (5.2)		7.6 (5.8)	

[a] from the intersection of absorption and emission; [b] from Equation (1); [c] from Equation (4); [d] from Equations (2) and (3); [e] from relative quantum yield measurements under Ar-purged conditions (see the Supporting Information); [f] intensity-weighted average lifetimes from time-correlated single-photon counting experiments in toluene under Ar-purged (unpurged) conditions (see the Supporting Information).

The small E_{re} of **DOBFT** and **DOBFIT** is a direct result of the small Δ_{BL}, as seen from the quantum chemical calculations, see Figure 3 and Table S5 (Supporting Information). In fact, most of the changes in bond lengths upon electronic excitation $|\Delta_{BL}|$ are smaller than 0.01 Å, and even the maximum $|\Delta_{BL}|$ is not larger than 0.03 Å. We then performed a full vibronic coupling calculation of the **DOBFT** and **DOBFIT** spectra. Applying a Gaussian broadening of γ_G = 0.07 eV, the calculated absorption and emission spectra agree well with experiment, see Figure 4. On the one hand, this confirms the reliability of the (TD)DFT-based Δ_{BL} calculations; on the other hand, it allows to disentangle the different contributions to the observed bandwidth. Focusing first in the low-energy region around F_1 (which determines FWHM), the FC broadening can be determined to be 0.08 eV (see the Experimental Section), so that we can conclude that linear coupling and environmental broadening (i.e., γ_G = 0.07 eV) have similar contributions to the FWHM. Since the minimum FWHM is very similar in **DABNA-1** (see analysis in Figure S11, Supporting Information) and other color-pure blue emitters,[12,25,51–54] this indicates that the coupling of low-frequency in-plane deformations of the core structure is apparently difficult to reduce further. On the other hand, this is different for the high-energy region, which gives rise to more visible vibronic side bands ($F_{2,3,...}$) of **DOBFT** and **DOBFIT** (Figure 4) compared to **DABNA-1** (Figure S2, Supporting Information), expressed in the smaller γ_E for the latter, see Table 1. This is directly correlated with the presence of a few somewhat elongated C—C bonds in the ground state of **DOBFT** and **DOBFIT** (Table S5, Supporting Information); indeed, the vibronic coupling analysis in Tables S7 and S9 (Supporting Information) proves significant coupling (with a Huang–Rhys factor of S = 0.04–0.07) for a few modes in the 1340–1450 cm^{-1} range, being more prominent compared with **DABNA-1** (Table S11, Supporting Information). Therefore, the use of the **OBP** motif in **DOBFT** and **DOBFIT** with its enriched structural versatility and color tuning, comes at the cost of inevitable broadening; nevertheless, the somewhat inferior behavior has no significant impact on color brilliance and hue.

Final crucial factors for the application in OLEDs are the fluorescence quantum yield Φ_F and lifetime τ_F. This is intrinsically provided by PHOD through the rigid core structure, and moderately high oscillator strengths f_{01}. In fact, in fluid solution (toluene, Ar-purged), we obtained Φ_F = 0.92 for **DOBFT**, see Table 1. The corresponding Φ_F is 8.1 ns; the latter permits some O_2 quenching under unpurged condition ($\tau_{F,air}$ = 6.2 ns). From Φ_F and τ_F, the radiative and nonradiative rates are calculated to be $k_r = \Phi_F/\tau_F = 1.1 \times 10^8$ s^{-1} and $k_{nr} = (1-\Phi_F)/\tau_F = 1.0 \times 10^7$ s^{-1}. The relatively small k_r is due to a moderate f_{01} of the transition (Table S4, Supporting Information),[55,56] which is, however, sufficient to compete effectively with the very low k_{nr}. The low

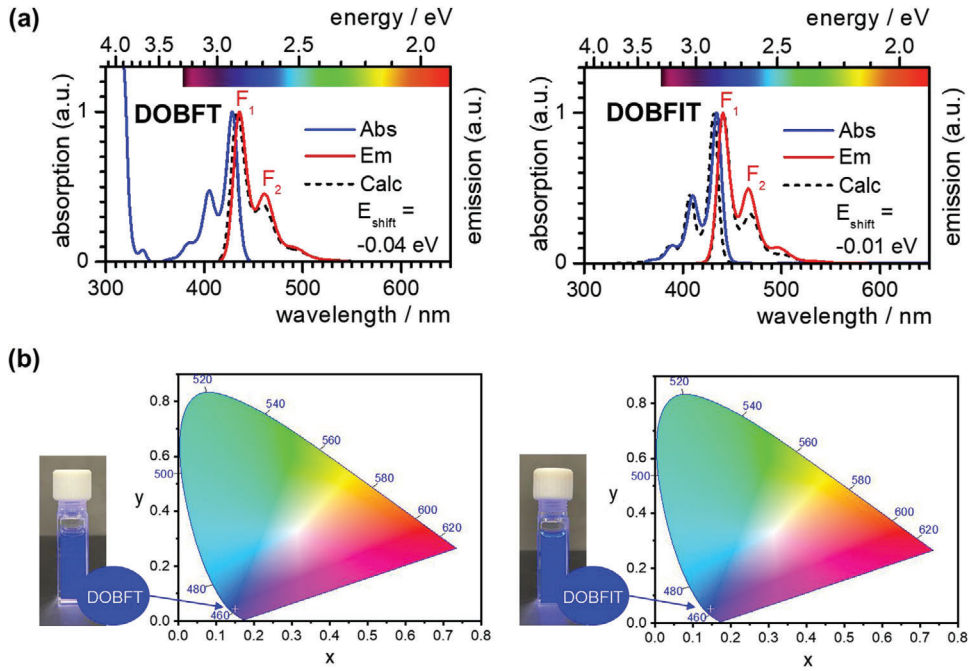

Figure 4. Optical properties of **DOBFT** and **DOBFIT**. a) Experimental absorption (blue) and emission (red) spectra, with calculated spectra in black (convoluted with a Gaussian of $\gamma_G = 0.07$ eV); b) CIE diagram, and fluorescence photograph upon UV irradiation under daylight.

k_{nr} reflects the rigidity of the core (suppressing IC and ISC) and the absence of heavy atom effects (minimizing ISC). Therefore, even under low temperature conditions, only very weak phosphorescence is observed, which is redshifted by −0.41 eV against fluorescence; see Figure S2 and Table S1 (Supporting Information). For **DOBFIT**, k_r amounts to 1.5×10^8 s^{-1}; which reflects a larger f_{01} of **DOBFIT** (Table S4, Supporting Information), and which reduces the lifetime to 6.3 ns, making **DOBFIT** less vulnerable against O_2 quenching, see Table 1. Finally, Φ_F amounts to 0.96, being very close to unity. In all, these properties make **DOBFT**, and even more **DOBFIT**, attractive candidates for OLED applications.

For potential application in OLEDs we performed preliminary tests, preparing films at 3 wt% doping ratio in PMMA and mCBP; all data are given in Figure S6 (Supporting Information). Both compounds maintain high Φ_F in the films (0.69 and 0.75 for **DOBFT** and **DOBFIT** in mCBP, respectively); this is equally reflected in only somewhat shortened τ_F compared to solution. The fluorescence spectra in both matrices are bathochromically shifted by a few nanometers compared to solution. At the same time, in all film spectra, the vibronic side bands are found to be enhanced, which points to specific host–guest interactions. The more intense side bands enlarge the FWHM by nearly a factor of three; however, the effective width γ_E (being in fact a more robust number) is much less affected, being larger by around 30% than those in solution. Nevertheless, the impact on the CIE coordinates is pronounced, deteriorating the color pureness in the films; this depends sensitively on compound and matrix (see Figure S7, Supporting Information).

The device characteristics for **DOBFIT** are reported in **Figure 5**, while the results for **DOBFT** (and **DABNA-1** for comparison) are found in Figures S8 and S9 (Supporting Information). The spectral response of **DOBFIT** approximately follows that of the solution and the thin film, concerning hue and FWHM; however, the external quantum efficiency (EQE) is relatively low. The latter effect is ascribed to the lack of TADF characteristics, as in related MR compounds; subsequently, higher EQE requires a more elaborated device architecture using sensitization through Coulomb-type energy transfer.[8–10] This, and further device optimization, are currently under investigation and will be reported in a forthcoming paper.

5. Conclusion

In conclusion, we have demonstrated the general recipe to generate color-pure blue and efficient emitters. This requires rigid core structures, where Clar sextets are co-annelated through BN or BO containing heteroaromatic rings; here, the large weight of zwitterionic resonance structures induces a strong reduction of bond length alternation; this effectively reduces the geometry change upon electronic excitation, which is responsible for spectral broadening by linear coupling of vibrational modes. This concept, termed as PHOD, is the common structural basis for DABNA-type emitters, relying on the **NBA** motif and its analogues. PHOD allowed to extend the accessible structural chemical space by further heteroaromatic motifs **NBP**, **OBP**. Based on our analysis, we have designed two novel emitters based on annelated **NBA**/**OBP** motifs with $\lambda_{vert} = 451$ nm ($\lambda_{max} = 436$ nm) for **DOBFT** and $\lambda_{vert} = 456$ nm ($\lambda_{max} = 441$ nm) for **DOBFIT**, and FWHM representing the lower expected limit of 0.11 eV (16 nm) and 0.09 eV (15 nm), respectively. The effective width was determined to $\gamma_E = 0.30$ and 0.29 eV, respectively, providing in all a brilliant hue of deep blue color with high fluorescence quantum

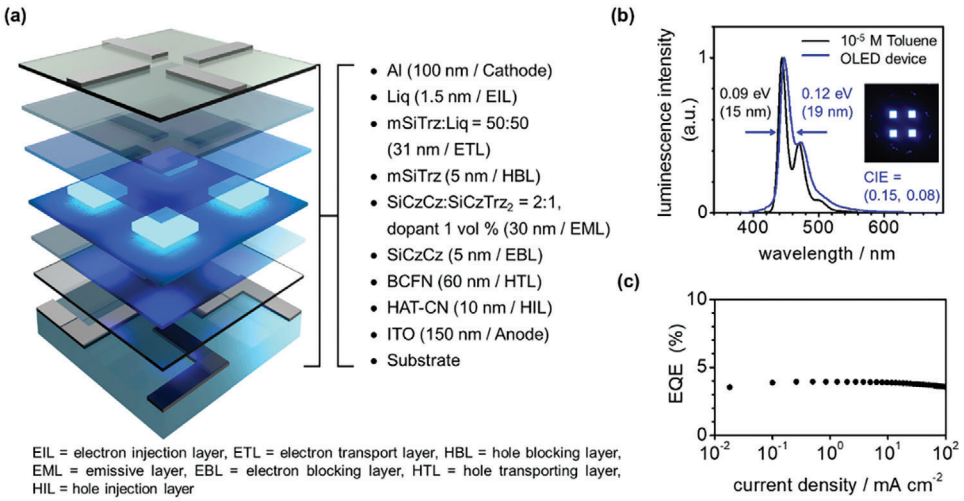

Figure 5. a) Stacked OLED device structure (for more details, see the Supporting Information); b) photoluminescence (PL) spectrum (with solution spectrum for comparison), and electroluminescence (EL) emission as inset with CIE coordinates; c) External quantum efficiency (EQE) vs current density characteristics.

yield Φ_F of 92% and 96%, and moderately short lifetimes τ_F of 8.1 and 6.3 ns, respectively.

In all, the simple and clear PHOD design rules promise rapid progress in the search for color-pure high-efficiency blue emitters with precisely tuned CIE coordinates, and their extension toward a wider spectral region. More fundamentally, PHOD provides a comprehensive interpretation of heteroaromatic systems in a broader context, extending beyond the current understanding of B,N-based heteroaromatics,[44,57,58] a concept not encompassed by the existing Clar's rule. This is anticipated to offer significant inspiration not only to researchers in the OLED field but also to those across various materials science disciplines.

6. Experimental Section

Synthesis: The novel compounds 7-(*tert*-butyl)−10-(4-(tert-butyl)phenyl)−10H-5,16-**dio**xa-10-aza-5a-**b**orafluoreno[3,2,1-gh]**t**etraphene (**DOBFT**) and 9-(*tert*-butyl)−6-(4-(tert-butyl)phenyl)−13,13-dimethyl-6,13-dihydro-11,19-**dio**xa-6-aza-10b-**b**orafluoreno[3,2,1-gh]indeno[1,2-l]**t**etraphene (**DOBFIT**) were synthesized by five-step reaction with a yield of 51% and 91%, respectively; details of the synthesis and characterization are given in the Supporting Information. **DABNA-1** was synthesized as described in literature.[12]

Spectroscopy and Data Analysis: The compounds were dissolved in toluene (spectroscopic grade), and purged with Ar. UV–vis absorption was recorded on a Cary 5000 UV–vis–NIR spectrometer (Varian). Fluorescence emission was obtained using a Jobin Yvon Fluorolog-3 spectrometer (HORIBA), and corrected for the sensitivity of the photomultiplier. Fluorescence decay times were recorded by time-correlated single photon counting (TCSPC; see the Supporting Information for details). To obtain the FC broadening contribution from the experimental FWHM (0.11 eV; see text), we use the additivity relation of variances upon convolution; using Equations (2) and (3), the FC width is extracted via $\gamma_{FC} = (\gamma_{FWHM}{}^2 - \gamma_{G2}{}^2)^{0.5}$ with $\gamma_{FWHM} = 0.11$ eV and $\gamma_G = 0.07$ eV to $\gamma_{FC} = 0.08$ eV.

Device Fabrication: The device structures were devices were fabricated using vacuum thermal evaporation. Further details regarding fabrication and structural characterization can be found in the Supporting Information. The EQE–J characteristics were assessed using a two-channel Source-Measure Unit (Keithley 2604b) alongside a calibrated photodiode (Thorlabs FDS1010-CAL). Electroluminescence (EL) spectra were acquired using a fiber-coupled, calibrated spectrometer (Ocean Optics FLAME-T-VIS-NIR).

Quantum Chemical Calculations: Ground and excited state optimization, MO analysis, vibrations, and single point time-dependent (TD) calculations were done at the DFT level, using the dispersion (D3)-corrected B3LYP functional and 6-311G* basis set with implicit solvent (toluene; PCM), as defined in the Gaussian 16 program package.[59] It is noted that, although standard DFT methods are not able to reproduce triplet state energies for MR-TADF compounds,[60] S_0 and S_1 geometries are expected to be well reproduced, as in fact shown in the current study. Vibronically resolved spectra were obtained using FCclasses3,[61] including thermal population at 298 K. A Gaussian broadening with a width of $\gamma_G = 0.07$ eV was applied to compare with experiment.

Bond Order and Bond Length: The value for a delocalized C—C bond d_{DLB} in the electronic ground state was obtained from DFT calculations of polyenes,[62] extracting averaged single (double) bonds d_{SB} (d_{DB}) of ≈1.45 Å (1.34 Å); with this, d_{DLB} gives 1.395 Å, and the range for delocalization (Figure 2) is set as 1.38 Å ≤ C—C ≤ 1.42 Å. From resonance theory, if all RS contribute equally, each C—C bond length is estimated by the abundance of double bond character x_{DB} in the different RS (see Figure 2 and Figure S2, Supporting Information). For a given bond, that is $x_{DB} = N_{DB}/N_{tot}$; this allows to calculate the bond length as $d = d_{DB}\cdot x_{DB} + d_{SB}\cdot(1-x_{DB})$. The resulting values for the C—C bonds agree reasonable with the DFT results not only for anthracene and phenanthrene, but also for NBA and OBP (see Table S2, Supporting Information); for both structures, this points to equal relevance of zwitterionic RS compared to the neutral ones.

The change in the bond length Δ_{BL} for a bond between atoms μ, ν upon electronic de-excitation $S_1 \rightarrow S_0$ can be obtained from bond order calculations in the corresponding states. In case that the transition corresponds mainly to a simple HOMO→LUMO excitation (as for the compounds under study), this gives $\Delta_{BL(\mu,\nu)} = c_{L,\mu}\cdot c_{L,\nu} - c_{H,\mu}\cdot c_{H,\nu}$, where c_L, c_H are the LCAO (linear combination of atomic orbitals) in the LUMO and HOMO orbitals, respectively. Therefore, an educative guess on Δ_{BL} can be directly obtained from simple frontier MO topology considerations, and Δ_{BL} will be large for strong changes in the bonding character in the FMOs for a given bond; see for instance the example of stilbene in Section 2.

Supporting Information

Supporting Information is available from the Wiley Online Library or from the author.

Acknowledgements

S.S., S.F., and L.W. contributed equally to this work. J.G. and B.M.-M. acknowledge funding from Spanish Ministerio de Ciencia e Innovación (MICIN-FEDER) project PID2022-138222NB-C21/22); R.W. acknowledges funding from MICIN-FEDER projects PID2021-128313OBI00 and TED2021-131018B-C22 and from the Comunidad de Madrid and the European Union structural funds through grant **S2018/NMT-4511**. The work in Madrid was additionally supported by the Severo Ochoa program for Centers of Excellence in R&D of the MICIN (**CEX2020-001039-S**) and by the Campus of International Excellence (CEI) UAM+CSIC. S.F. acknowledges a grant from the China Scholarship Council (CSC; grant no. **202008330343**). M.S.K. acknowledges support from LG chemistry, and the National Research Foundation of Korea (NRF) funded by the Korean government (MSIT; grant no. **2022R1A2C2011627 and 2021R1A5A1030054**). J. L and J. J were financially supported by Samsung Display Co., Ltd. [Correction added on August 2, 2024, after first online publication: Figure 4 has been corrected.]

Conflict of Interest

The authors declare no conflict of interest.

Data Availability Statement

The data that support the findings of this study are available in the supplementary material of this article.

Keywords

blue emitter, color pureness, color-pure OLED, fluorescence, vibronic coupling

Received: March 26, 2024
Revised: June 21, 2024
Published online: July 16, 2024

[1] S. M. Suresh, D. Hall, D. Beljonne, Y. Olivier, E. Zysman-Colman, *Adv. Funct. Mater.* **2020**, *30*, 1908677.
[2] S. S. Kothavale, J. Y. Lee, *Adv. Opt. Mater.* **2020**, *8*, 2000922.
[3] H. Lee, D. Karthik, R. Lampande, J. H. Ryu, J. H. Kwon, *Front. Chem.* **2020**, *8*, 373.
[4] J. M. Ha, S. H. Hur, A. Pathak, J.-E. Jeong, H. Y. Woo, *NPG Asia Mater.* **2021**, *13*, 53.
[5] M. Xie, M. Sun, S. Xue, W. Yang, *Dyes Pigm.* **2023**, *208*, 110799.
[6] C. Lv, X. Wang, Q. Zhang, Y. Zhang, *Mater. Chem. Front.* **2023**, *7*, 2809.
[7] H. Jiang, J. Jin, W. Y. Wong, *Adv. Funct. Mater.* **2023**, *33*, 2306880.
[8] C.-Y. Chan, M. Tanaka, Y.-T. Lee, Y.-W. Wong, H. Nakanotani, T. Hatakeyama, C. Adachi, *Nat. Photonics* **2021**, *15*, 203.
[9] S. K. Behera, R. D. Costa, *J. Mater. Chem.* **2023**, *11*, 13647.
[10] Y. Gawale, R. Ansari, K. R. Naveen, J. H. Kwon, *Front. Chem.* **2023**, *11*, 1211345.
[11] G. K. J. Chen, J. Chen, in *Handbook of Visual Display Technology*, (Eds: J. Chen, W. Cranton, M. Fihn), Springer, Cham **2016**, pp. 1779–1797.
[12] T. Hatakeyama, K. Shiren, K. Nakajima, S. Nomura, S. Nakatsuka, K. Kinoshita, J. Ni, Y. Ono, T. Ikuta, *Adv. Mater.* **2016**, *28*, 2777.
[13] Y. Kondo, K. Yoshiura, S. Kitera, H. Nishi, S. Oda, H. Gotoh, Y. Sasada, M. Yanai, T. Hatakeyama, *Nat. Photonics* **2019**, *13*, 678.
[14] a) H. Hirai, K. Nakajima, S. Nakatsuka, K. Shiren, J. Ni, S. Nomura, T. Ikuta, T. Hatakeyama, *Angew. Chem., Int. Ed.* **2015**, *54*, 13581; b) J. Park, J. Lim, J. H. Lee, B. Jang, J. H. Han, S. S. Yoon, J. Y. Lee, *ACS Appl. Mater. Interfaces* **2021**, *13*, 45798.
[15] Y. Yuan, X. Tang, X. Y. Du, Y. Hu, Y. J. Yu, Z. Q. Jiang, L. S. Liao, S. T. Lee, *Adv. Opt. Mater.* **2019**, *7*, 1801536.
[16] B. R. Henry, W. Siebrand, in *Organic Molecular Photophysics*, (Ed: J. B. Birks), Wiley, New York **1973**, pp. 153–237.
[17] C. Manneback, *Physica* **1951**, *17*, 1001.
[18] W. Siebrand, *J. Chem. Phys.* **1967**, *46*, 440.
[19] F. Negri, M. Z. Zgierski, *J. Chem. Phys.* **1994**, *100*, 2571.
[20] J. Gierschner, H.-G. Mack, L. Lüer, D. Oelkrug, *J. Chem. Phys.* **2002**, *116*, 8596.
[21] M. Eskandari, J. C. Roldao, J. Cerezo, B. Milian-Medina, J. Gierschner, *J. Am. Chem. Soc.* **2020**, *142*, 2835.
[22] W. Cai, C. Zhong, D.-Y. Wu, *Mater. Chem. Front.* **2023**, *7*, 3762.
[23] S. A. Ahmad, J. Eng, T. J. Penfold, *J. Mater. Chem. C* **2022**, *10*, 4785.
[24] a) X. Ye, L. Xu, F. Qiu, Z. Ma, B. Wang, J. Zhou, S. Xiong, Y. Ma, D. Hu, G. Tian, *Energy Fuels* **2021**, *35*, 19139; b) H. Zhang, L. Ke, Z. Li, Y. Nie, J. Wang, H. Bi, Y. Wang, *J. Mater. Chem.* **2023**, *11*, 9300.
[25] H. Lee, R. Braveenth, J. D. Park, C. Y. Jeon, H. S. Lee, J. H. Kwon, *ACS Appl. Mater. Interfaces* **2022**, *14*, 36927.
[26] a) J. C. Sancho Garcia, J. L. Brédas, D. Beljonne, J. Cornil, R. Martinez Alvarez, M. Hanack, L. Poulsen, J. Gierschner, H.-G. Mack, H.-J. Egelhaaf, D. Oelkrug, *J. Phys. Chem. B* **2005**, *109*, 4872; b) J. Gierschner, H.-G. Mack, D. Oelkrug, I. Waldner, H. Rau, *J. Phys. Chem. A* **2004**, *108*, 257.
[27] J. Arago, P. M. Viruela, J. Gierschner, E. Orti, B. Milian-Medina, *Phys. Chem. Chem. Phys.* **2011**, *13*, 1457.
[28] a) B. M. Medina, D. Wasserberg, S. C. Meskers, E. Mena-Osteritz, P. Bäuerle, J. Gierschner, *J. Phys. Chem. A* **2008**, *112*, 13282; b) G. Heimel, M. Daghofer, J. Gierschner, E. J. List, A. C. Grimsdale, K. Mullen, D. Beljonne, J. L. Bredas, E. Zojer, *J. Chem. Phys.* **2005**, *122*, 054501.
[29] a) J. Gierschner, H. G. Mack, H. J. Egelhaaf, S. Schweizer, B. Doser, D. Oelkrug, *Synth. Met.* **2003**, *138*, 311; b) G. Macchi, B. M. Medina, M. Zambianchi, R. Tubino, J. Cornil, G. Barbarella, J. Gierschner, F. Meinardi, *Phys. Chem. Chem. Phys.* **2009**, *11*, 984.
[30] G. Srinivasan, J. A. Villanueva-Garibay, K. Müller, D. Oelkrug, B. Milian Medina, D. Beljonne, J. Cornil, M. Wykes, L. Viani, J. Gierschner, R. Martinez-Alvarez, M. Jazdzyk, M. Hanack, H. J. Egelhaaf, *Phys. Chem. Chem. Phys.* **2009**, *11*, 4996.
[31] J. Cerezo, J. Gierschner, F. Santoro, G. Prampolini, *ChemPhysChem* **2024**, *25*, 202400307.
[32] a) M. Wykes, R. Parambil Mangattu, D. Beljonne, J. Gierschner, *J. Chem. Phys.* **2015**, *143*, 114116; b) M. Wykes, S. K. Park, S. Bhattacharyya, S. Varghese, J. E. Kwon, D. R. Whang, I. Cho, R. Wannemacher, L. Lüer, S. Y. Park, J. Gierschner, *J. Phys. Chem. Lett.* **2015**, *6*, 3682; c) M. J. Aliaga-Gosalvez, M. Demitri, M. Dohr, J. C. Roldao, S. K. Park, S. Oh, S. Varghese, S. Oh, S. Y. Park, Y. Olivier, B. Milián-Medina, R. Resel, J. Gierschner, *Adv. Opt. Mater.* **2019**, *7*, 1900749.
[33] J. Gierschner, J. Cornil, H. J. Egelhaaf, *Adv. Mater.* **2007**, *19*, 173.
[34] F. Santoro, J. A. Green, L. Martinez-Fernandez, J. Cerezo, R. Improta, *Phys. Chem. Chem. Phys.* **2021**, *23*, 8181.
[35] a) H.-H. Perkampus, *UV-Vis Atlas of Organic Compounds*, Wiley, New York **1996**; b) M. Klessinger, J. Michl, *Excited States and Photochemistry of Organic Molecules*, Wiley, New York **1995**, pp. 18–20, 71–76.
[36] N. Nijegorodov, V. Ramachandran, D. P. Winkoun, *Spectrochim. Acta, Part A* **1997**, *53*, 1813.
[37] It is noted in this context that the 1LA state in anthracene (S0→S1 transition) and phenanthrene (S0→S2; while S0→S1 corresponds to 1LA; see, e.g. ref. [35b]) shows considerable configuration interaction, and thus cannot be solely described by a HOMO→LUMO excitation; therefore, also the simple consideration of frontier MO topologies for an educative guess on ΔBL cannot be applied.
[38] T. Suzuki, N. Mikami, M. Ito, *J. Phys. Chem.* **1986**, *90*, 6431.

[39] K. Klehs, C. Spahn, U. Endesfelder, S. F. Lee, A. Fürstenberg, M. Heilemann, *ChemPhysChem* **2014**, *15*, 637.
[40] E. Heilbronner, H. Bock, *The HMO Model and Its Application. Part 1. Basis and Manipulation*, John Wiley – Verlag Chemie, London, Weinheim **1976**.
[41] a) E. Clar, *The Aromatic Sextet*, Wiley, London **1972**; b) M. Sola, *Front. Chem.* **2013**, *1*, 22.
[42] L. Pauling, *The Nature of the Chemical Bond*, 3rd ed. Cornell University Press, New York **1960**, pp. 198–201.
[43] G. M. Badger, *The Structure and Reactions of Aromatic Compounds*, Cambridge University Press, Cambridge **1954**.
[44] A. Abengózar, P. García-García, M. A. Fernández-Rodríguez, D. Sucunza, J. J. Vaquero, *Adv. Heterocycl. Chem.* **2022**, *135*, 197.
[45] K. Stavrou, S. Madayanad Suresh, D. Hall, A. Danos, N. A. Kukhta, A. M. Z. Slawin, S. Warriner, D. Beljonne, Y. Olivier, A. Monkman, E. Zysman-Colman, *Adv. Opt. Mater.* **2022**, *10*, 2200688.
[46] a) S. Wu, L. Zhang, J. Wang, A. Kumar Gupta, I. D. W. Samuel, E. Zysman-Colman, *Angew. Chem., Int. Ed.* **2023**, *62*, 202305182; b) G. Wang, S. Ding, J. Li, X. Li, W. Xia, X. Chen, H. Yao, Z. Ye, K. Zhang, *Chem. Mater.* **2024**, *36*, 3000.
[47] M. J. S. Dewar, V. P. Kubba, R. Pettit, *J. Chem. Soc.* **1958**, 3073.
[48] M. J. S. Dewar, R. Dietz, *J. Chem. Soc.* **1960**, 1344.
[49] S. Asano, H. N. Tanaka, A. Imamura, H. Ishida, H. Ando, *Org. Lett.* **2019**, *21*, 4197.
[50] S. H. Han, J. H. Jeong, J. W. Yoo, J. Y. Lee, *J. Mater. Chem.* **2019**, *7*, 3082.
[51] K. Matsui, S. Oda, K. Yoshiura, K. Nakajima, N. Yasuda, T. Hatakeyama, *J. Am. Chem. Soc.* **2018**, *140*, 1195.
[52] S. Oda, W. Kumano, T. Hama, R. Kawasumi, K. Yoshiura, T. Hatakeyama, *Angew. Chem., Int. Ed.* **2021**, *60*, 2882.
[53] B. Lei, Z. Huang, S. Li, J. Liu, Z. Bin, J. You, *Angew. Chem., Int. Ed.* **2023**, *62*, 202218405.
[54] S. M. Suresh, L. Zhang, T. Matulaitis, D. Hall, C. Si, G. Ricci, A. M. Z. Slawin, S. Warriner, D. Beljonne, Y. Olivier, I. D. W. Samuel, E. Zysman-Colman, *Adv. Mater.* **2023**, *35*, 2300997.
[55] S. J. Strickler, R. A. Berg, *J. Chem. Phys.* **1962**, *37*, 814.
[56] J. Gierschner, J. Shi, B. Milián-Medina, D. Roca-Sanjuán, S. Varghese, S. Park, *Adv. Opt. Mater.* **2021**, *9*, 2002251.
[57] P. G. Campbell, A. J. V. Marwitz, S.-Y. Liu, *Angew. Chem., Int. Ed.* **2012**, *51*, 6074.
[58] H. Helten, *Chemistry* **2016**, *22*, 12972.
[59] M. J. Frisch, G. W. Trucks, H. B. Schlegel, G. E. Scuseria, M. A. Robb, J. R. Cheeseman, G. Scalmani, V. Barone, G. A. Petersson, H. Nakatsuji, X. Li, M. Caricato, A. V. Marenich, J. Bloino, B. G. Janesko, R. Gomperts, B. Mennucci, H. P. Hratchian, J. V. Ortiz, A. F. Izmaylov, J. L. Sonnenberg, D. Williams-Young, F. Ding, F. Lipparini, F. Egidi, J. Goings, B. Peng, A. Petrone, T. Henderson, D. Ranasinghe, et al., *Gaussian 16, Revision C.01*, Gaussian Inc, Wallingford, CT **2016**.
[60] D. Hall, J. C. Sancho-Garcia, A. Pershin, G. Ricci, D. Beljonne, E. Zysman-Colman, Y. Olivier, *J. Chem. Theory Comput.* **2022**, *18*, 4903.
[61] J. Cerezo, F. Santoro, *J. Comput. Chem.* **2023**, *44*, 626.
[62] T. Kupka, A. Buczek, M. A. Broda, M. Stachow, P. Tarnowski, *J. Mol. Model.* **2016**, *22*, 101.